

N3P: Accelerated Automated Parking via a Learning-Based Naturalistic Three-Stage Scheme

Yifan Xue^{1,2}, Toktam Mohammadnejad¹, Faizan M Tariq¹, Sangjae Bae¹, David Isele¹,
Yosuke Sakamoto¹, Nadia Figueroa², Jovin D’sa¹

Abstract—Autonomous parking requires efficient path planning that ensures kinematic feasibility and collision avoidance in constrained environments. Hybrid A* is widely used but computationally expensive, while reinforcement learning (RL) methods lack reliability and often struggle with long-horizon geometric constraints, leading to suboptimal trajectories. We present N3P, a fast learning-based three-stage framework for automated parking. By introducing an intermediate preparatory pose and using a learning module to predict it, N3P decomposes the maneuver into simpler subproblems, thereby reducing computational complexity and accelerating path generation. We validate the framework by integrating it with Hybrid A* algorithms. Experiments in perpendicular and parallel parking scenarios show that N3P-enhanced Hybrid A* speeds up planning by more than 80%. It also outperforms RL baselines in success rate and trajectory quality, producing shorter trajectories with fewer gear changes, while achieving comparable or lower planning time in most cases.

I. INTRODUCTION

Autonomous parking is an important Driver Assistance function in modern cars. For autonomous parking to perform well in real life, we need algorithms to generate kinematically feasible, collision-free paths. Ideally, such an algorithm should provide low-latency planning suitable for practical parking scenarios with tight spatial constraints.

Graph-search and optimization-based algorithms are among the most widely used approaches for autonomous parking path planning. Classical graph-search methods such as A* and Rapidly-exploring Random Trees (RRT) guarantee theoretical completeness, but cannot ensure kinematic feasibility of the resulting path [1]–[4]. Hybrid A* addresses this by incorporating motion primitives that satisfy nonholonomic constraints, often augmented with analytic expansions using Reeds-Shepp curves to improve accuracy and reduce node expansion [5]–[7]. Nevertheless, in tightly constrained parking scenarios, Hybrid A* and its sped-up variants still require extensive node expansions and rarely achieve sub-second runtimes [8]–[10]. Optimization-based methods generate smooth, dynamically feasible, and cost-efficient trajectories. However, they are susceptible to convergence to local minima [11]–[13] and often require several seconds—or even minutes—to converge, even when a globally optimal solution exists. To mitigate local minima issues inherent in nonlinear path optimization, popular approaches initialize optimization [11], [14]–[16] or construct convex

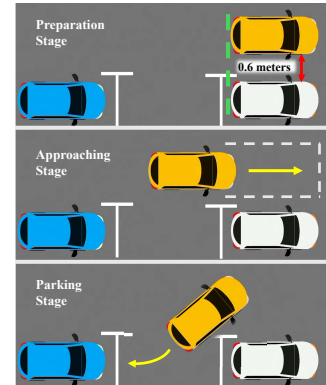


Fig. 1: During parking, human drivers often follow a preparation phase to select an intermediate pose, an approaching phase to reach it, and a parking phase to complete the maneuver. N3P adopts this strategy, using an offline-learned model to select preparatory poses and accelerate planning.

corridors from nonconvex obstacle constraints [17] using coarse trajectories generated by Hybrid A*. Consequently, graph-search computation remains a major contributor to the overall runtime bottleneck in such optimization frameworks.

More recently, learning-based methods have been proposed, leveraging deep neural networks [18]–[20] and reinforcement learning (RL) [21]–[23] to handle highly constrained parking. Although these methods are fast at inference, their performance depends strongly on the quality, diversity, and coverage of training data, and distributional shifts can significantly degrade reliability. In addition, learned policies typically do not enforce explicit recursive feasibility, which can lead to failure in reaching the goal and aggressive near-collision maneuvers, reducing passenger comfort. These limitations motivate exploring alternative approaches that combine human-inspired strategies with structured planners.

Unlike traditional autonomous path planners, which exhaustively explore all possible trajectories from the vehicle’s current pose to the parking spot to find an optimal path, human drivers often follow a more efficient three-stage strategy as illustrated in Fig. 1. In the first *preparation stage*, drivers identify an intermediate pose near the target parking spot that facilitates an easier final maneuver. In the second *approaching stage*, they maneuver the vehicle into this preparatory pose. Finally, in the third *parking phase*, they execute a smooth, continuous motion from the preparatory pose into the parking spot. Motivated by this behavior, we propose N3P, a naturalistic three-stage parking scheme that uses an offline-learned model to select preparatory poses

¹Honda Research Institute (HRI), Mountain View, CA. ²University of Pennsylvania, PA. The work was done during Yifan Xue’s internship at HRI. (Email: toktam.mohammadnejad@honda-ri.com, jovin.dsa@honda-ri.com, & yifanxue@seas.upenn.edu.)

during planning, accelerating the overall process.

Dividing complex path planning problems into smaller subproblems is not new in parking control architecture design. For example, [24] decomposes MPC-based planning into sequential traversal of three predefined rectangular corridors, while [25] analytically computes a preparatory pose for forward and parallel parking based on vehicle geometry and steering limits. However, these approaches do not scale well to complex valet parking scenarios. The corridor structure in [24] is validated only on one perpendicular and one parallel parking case with manually designed corridors, and it is unclear how such corridors should be adapted to varying initial poses and environments. Although [25] improves generalization, it is still restricted by the limited representational capacity of analytical methods in environments with spacious, obstacle-free lanes. This limitation prevents its application in real-world valet parking settings with irregular layouts and surrounding vehicles.

The contributions of the paper are summarized as follows:

- A naturalistic three-stage parking framework that reduces computation complexity of parking path planning via a learned preparatory pose selector.
- A scalable offline-to-online abstraction pipeline that enables a learned preparatory pose selector, trained on simplified environments, to generalize to realistic cluttered parking scenes.

To evaluate N3P in a representative and widely adopted setting, we integrate it within Hybrid A*, which is commonly used both as a standalone planner and as an initialization for optimization-based control. The resulting N3P-enhanced Hybrid A* is compared against existing Hybrid A* variants and HOPE [23], a transformer-based RL agent, using randomly generated parking scenarios that emulate real-world challenges such as tight maneuvering spaces and dead ends.

II. PROBLEM FORMULATION

A. Environment Construction

Without loss of generality, we formulate the problem in a parking-spot-based frame \hat{p} , where the parking spot center is set as the origin, as illustrated in Fig. 2. The coordinate system is defined such that the positive x -axis aligns with the drive lane and points toward the vehicle's goal heading for parallel parking, while the positive y -axis points from the parking spot toward the drive lane. We denote the parking goal poses as $\mathbf{g}^{\hat{p}}$.

B. Vehicle Model

Let (x, y, θ) be the autonomous vehicle state, where x, y are the 2D positions in meters and θ is the angle between the vehicle heading and the positive x -axis in radians. We employ the kinematic bicycle model for vehicle dynamics, which is well-suited for vehicles at low speeds [26] and has been widely used in similar autonomous parking applications [5], [8], [10], [23], [27].

$$\dot{\mathbf{x}} = \begin{bmatrix} \dot{x} \\ \dot{y} \\ \dot{\theta} \end{bmatrix} = \begin{bmatrix} v \cos \theta \\ v \sin \theta \\ \frac{v}{l} \tan \delta \end{bmatrix} \quad (1)$$

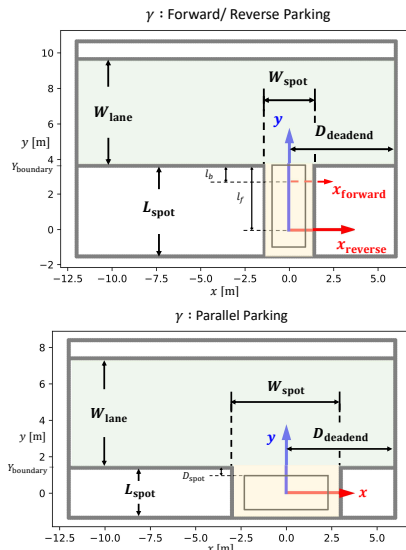


Fig. 2: Examples of parking-spot-based frames \hat{p} for forward, reverse, and parallel parking. Drive lanes are shown in green and parking spots in yellow.

Here l is the wheelbase of the vehicle, approximated as a rectangle. $u = [v, \delta]^T$ is the control input, where v is the longitudinal velocity and δ is the steering angle of the front wheel. The control inputs are subject to box constraints: $v \in [v_{\min}, v_{\max}]$ and $\delta \in [\delta_{\min}, \delta_{\max}]$.

C. Reeds-Shepp Path

Reeds and Shepp [28] proved that, in an obstacle-free environment, the shortest path between planar configurations (x, y, θ) for a bidirectional vehicle with bounded curvature $\kappa = \tan(\delta_{\max})/l$ consists of a finite sequence of straight segments (S) and maximum-curvature arcs (L for left turns and R for right turns). Such trajectories are commonly referred to as Reeds-Shepp (RS) paths. In environments with obstacles, collision-free RS paths are obtained by generating candidate RS curves between the initial and goal configurations and performing collision checking on each trajectory. Due to its analytical tractability and ability to model bidirectional motion, RS paths are widely used as a local connection strategy in autonomous parking algorithms.

D. Path Planning Problem Definition

We assume the autonomous vehicle has access to detectable obstacle point clouds along the path from its initial position to the parking target. The scope of this work focuses on **perpendicular** (forward and reverse) and **parallel** parking scenarios, but this approach could be extended to include additional parking types such as angled parking.

Problem Statement: Given the initial state $\mathbf{x}_0^{\hat{p}}$ of the ego vehicle, and obstacle point clouds in the parking environment, the goal is to find a sequence of control inputs u that satisfy the kinematic model in Eq. 1 and the actuation limits, steering the vehicle to the desired parking pose $\mathbf{g}^{\hat{p}} \in \mathbb{R}^3$ while avoiding obstacle collisions and yielding a path of short trajectory length, few gear changes and few steering angle changes.

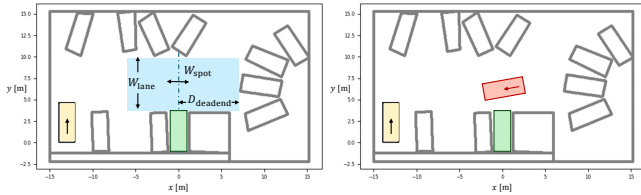


Fig. 3: Left: extraction of abstracted parameters from an arbitrary environment under valid parking conditions. Right: an invalid scenario where another vehicle blocks the rectangular access region of the target parking space.

III. METHODOLOGY OVERVIEW

Inspired by how human drivers use a preparatory pose to simplify parking into intuitive steps, the N3P framework we propose similarly consists of three stages:

- Preparation stage: Given an arbitrary parking environment, abstract the region surrounding the goal parking pose into a local configuration \mathcal{E} and determine a feasible preparatory pose $\mathbf{g}_{\text{pre}}^{\hat{p}} \in \mathbb{R}^3$ based on this abstraction.
- Approaching stage: Solve for a path from the initial vehicle state $\mathbf{x}_0^{\hat{p}}$ to the preparatory pose $\mathbf{g}_{\text{pre}}^{\hat{p}}$ using a graph-search or optimization-based parking planner.
- Parking stage: Compute an optimal parking maneuver from the preparatory pose $\mathbf{g}_{\text{pre}}^{\hat{p}}$ to the parking goal $\mathbf{g}^{\hat{p}}$ using an analytical Reeds–Shepp path.

Selecting preparatory poses faces three key challenges. First, parking environments vary in spot dimensions, infrastructure geometry, and surrounding vehicles, creating effectively unlimited scenarios. Abstracting these diverse conditions into a finite set that can be handled with limited offline data and training is nontrivial. Second, poorly selected intermediate poses can degrade path quality, resulting in longer trajectories or more direction changes. Third, ensuring feasibility is challenging: although planning from $\mathbf{x}_0^{\hat{p}}$ to $\mathbf{g}_{\text{pre}}^{\hat{p}}$ is typically more efficient than planning directly to $\mathbf{g}^{\hat{p}}$, the subsequent connection from $\mathbf{g}_{\text{pre}}^{\hat{p}}$ to $\mathbf{g}^{\hat{p}}$ may still be computationally expensive or even infeasible under kinematic and environmental constraints. In the following sections, we describe how the N3P framework addresses these challenges. Section IV presents how diverse parking environments are abstracted into a finite set of representative configurations. Section V describes how offline data generation and model training produce preparatory poses that allow smooth and easily executed maneuvers to the parking goal. Finally, Section VI explains the online deployment of the learned preparatory pose selector for accelerated path planning in realistic parking scenarios.

IV. ENVIRONMENT ABSTRACTION

Obstacle distributions near a parking goal vary widely, making it impractical to explicitly model all possible configurations or train a preparatory pose selector that accounts for every geometric detail. Rather than attempting exhaustive coverage of obstacle layouts, we instead identify the geometric conditions that fundamentally determine the type

of maneuver required. As shown in Fig. 3, we observe that a parking goal is feasible only if a sufficiently large obstacle-free rectangular region exists on the drive lane adjacent to the parking spot. The size and relative position of this free-space rectangle directly determines the maneuver strategy, for example, whether ample approach space is available or whether constrained, multi-switch maneuvers are necessary. Therefore, instead of representing full obstacle configurations, we abstract each environment by the geometry of its largest feasible free-space rectangle. Under this abstraction, two environments are considered equivalent for preparatory pose selection if they share the same free-space rectangle dimensions and relative positioning under the same parking type. This reduction enables us to exhaustively cover all geometrically distinct maneuver conditions using only four parameters: lane width W_{lane} , spot width W_{spot} , dead-end depth D_{deadend} , and parking type γ (forward, reverse, or parallel), as in Fig. 2.

$$\mathcal{E} = \{W_{\text{lane}}, W_{\text{spot}}, D_{\text{deadend}}, \gamma\} \quad (2)$$

The parking type γ is assumed known from the parking-spot geometry prior to local planning. When the parking lane does not have a nearby dead end, D_{deadend} is the distance from the center of the vehicle parking spot to the boundary of our local parking environment. The parking spot length L_{spot} is not used to describe the parking infrastructure because autonomous vehicles do not need this information to determine their parking poses. In the perpendicular parking scenarios, once the vehicle finds a path to the poses shown in Fig. 2, it can easily adjust itself to the desired depth inside the parking spot by simply moving forward or backward in a straight line. In parallel parking scenarios, any final parking pose is considered appropriate as long as it leaves a sufficient depth D_{spot} from the boundary Y_{boundary} between the parking spot and the lane.

V. PREPARATORY POSE SELECTOR

A good preparatory pose $\mathbf{g}_{\text{pre}}^{\hat{p}}$ in parking navigation should satisfy two requirements: (1) there must exist a kinematically feasible and collision-free trajectory from the vehicle’s initial state $\mathbf{x}_0^{\hat{p}}$ to $\mathbf{g}_{\text{pre}}^{\hat{p}}$, and (2) it should be straightforward to generate a smooth connecting path from $\mathbf{g}_{\text{pre}}^{\hat{p}}$ to the final parking pose $\mathbf{g}^{\hat{p}}$. To satisfy the second requirement, we consider RS paths, which naturally capture the multi-segment forward–reverse maneuvers required in parking and enable real-time closed-form evaluation of the connecting trajectory. The remaining challenge is to identify start poses that admit collision-free RS connections to $\mathbf{g}^{\hat{p}}$ while also being reachable from the initial state $\mathbf{x}_0^{\hat{p}}$. A straightforward approach is to uniformly sample configurations around the parking spot and evaluate their connections. However, since RS paths are defined over a continuous configuration space, valid connecting configurations are typically confined to a narrow subset of states, making them difficult to reliably discover through discrete sampling, even at fine resolutions.

Here, we novelly select the **starting pose of the RS curve** $\mathbf{x}_{\text{rs}}^{\hat{p}}$ generated by the RS-augmented Hybrid A* as exemplary

preparatory poses for parking applications [5]. Since $\mathbf{x}_{\text{rs}}^{\hat{p}}$ is a point on the drivable Hybrid A* path computed, it trivially ensures a kinematically feasible and collision-free path to $\mathbf{x}_0^{\hat{p}}$, as well as to $\mathbf{g}^{\hat{p}}$.

A. Offline Data Collection

We categorize parking scenarios by environment parameters \mathcal{E} and construct a collective set \mathbb{E} :

$$\mathbb{E} = \{\mathcal{E} | \forall W_{\text{lane}} \in \mathcal{W}_{\text{lane}}, W_{\text{spot}} \in \mathcal{W}_{\text{spot}}, D_{\text{deadend}} \in \mathcal{D}_{\text{deadend}}, \gamma \in \Gamma_{\text{type}}\}, \quad (3)$$

where \mathcal{E} is single parking scenario defined as in Eq. 2, and $\mathcal{W}_{\text{lane}}$, $\mathcal{W}_{\text{spot}}$, and $\mathcal{D}_{\text{deadend}}$ denote the discretized sets of drive-lane width, parking-spot width, and dead-end length, respectively. Each set is uniformly sampled within a predefined range with a fixed resolution, reflecting typical dimensions in real-world parking structure designs.

$$\begin{aligned} \mathcal{W}_{\text{lane}} &= \left\{ w^{(l)} \mid i \in \mathbb{N}, w^{(l)} = w_{\min}^{(l)} + i\Delta w^{(l)} \leq w_{\max}^{(l)} \right\}, \\ \mathcal{W}_{\text{spot}} &= \left\{ w^{(s)} \mid i \in \mathbb{N}, w^{(s)} = w_{\min}^{(s)} + i\Delta w^{(s)} \leq w_{\max}^{(s)} \right\}, \\ \mathcal{D}_{\text{deadend}} &= \{d \mid i \in \mathbb{N}, d = d_{\min} + i\Delta d \leq d_{\max}\}, \\ \gamma \in \Gamma_{\text{type}} &= \{\text{“forward”}, \text{“reverse”}, \text{“parallel”}\}. \end{aligned} \quad (4)$$

Here, $(w_{\min}^{(s)}, w_{\max}^{(s)})$, $(w_{\min}^{(l)}, w_{\max}^{(l)})$, (d_{\min}, d_{\max}) are respectively the range of W_{lane} , W_{spot} , D_{deadend} to be considered and $\Delta w^{(s)}$, $\Delta w^{(l)}$, Δd are corresponding resolutions. The environment simplification in Section IV enables representing obstacle conditions with only three parameters— W_{lane} , W_{spot} , and D_{deadend} . By uniformly sampling within defined parameter ranges, the data are guaranteed to represent all distinctive environments of interest with controllable granularity. Such completeness cannot be ensured by high-dimensional environment representations based on obstacle configurations or LiDAR distance vectors. Although the parameter ranges must be specified by the user, the calibration burden is minimal, as they can be readily determined from local regulations on lane widths and parking spot dimensions.

For each parking scenario in \mathbb{E} , we repeatedly solve the Hybrid A* augmented with RS paths offline using initial states $\tilde{\mathbf{x}}_0^{\hat{p}}$ uniformly sampled in the free space of the abstracted environments. The starting poses $\tilde{\mathbf{x}}_{\text{rs}}^{\hat{p}}$ of the RS segments in the resulting drivable trajectories are stored in the set $\tilde{\mathcal{X}}_{\text{rs}}^{\hat{p}}[\mathcal{E}] \in \mathbb{R}^{N_{\mathcal{E}} \times 3}$, with their corresponding initial states $\tilde{\mathbf{x}}_0^{\hat{p}}$ stored in $\tilde{\mathcal{X}}_0^{\hat{p}}[\mathcal{E}] \in \mathbb{R}^{N_{\mathcal{E}} \times 3}$, where $N_{\mathcal{E}}$ is the number of data samples collected for parking environment \mathcal{E} . Examples of collected $\tilde{\mathcal{X}}_{\text{rs}}^{\hat{p}}[\mathcal{E}]$ can be found in Fig. 4.

B. Learning-Based Models

In the learning-based model, we trained models using collected RS starting poses $\tilde{\mathcal{X}}_{\text{rs}}^{\hat{p}}$, vehicle initial states $\tilde{\mathcal{X}}_0^{\hat{p}}$ and the environment parameters \mathbb{E} corresponded to them. Given the vehicle’s initial states $\mathbf{x}_0^{\hat{p}}$ and the parking environment \mathcal{E} , as inputs, the goal of our learned preparatory pose selector $f_{\gamma}(\cdot)$ can be formally summarized as follows:

$$\mathbf{g}_{\text{pre}}^{\hat{p}}(\mathbf{x}_0^{\hat{p}}, \mathcal{E}) = f_{\gamma}(\mathbf{x}; \mathbf{w}), \quad (5)$$

$$\mathbf{x} = [x_0^{\hat{p}}, y_0^{\hat{p}}, \theta_0^{\hat{p}}, W_{\text{lane}}, W_{\text{spot}}, D_{\text{deadend}}]^{\top}, \quad (6)$$

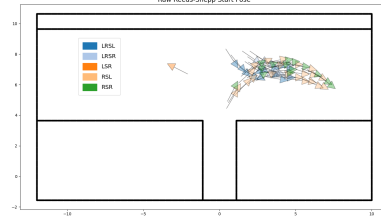


Fig. 4: Reeds–Shepp start poses for the reverse parking environment \mathcal{E} , colored by curve type to the goal: “S” for straight, “R”/“L” for right/left arcs.

where $\mathbf{x} \in \mathbb{R}^6$ is the input, \mathbf{w} is the parameter vector, and $\mathbf{g}_{\text{pre}}^{\hat{p}}$ is the preparatory pose output of the model. The model $f_{\gamma}(\mathbf{x}; \mathbf{w})$ is trained using input features $\mathbf{X}_{\text{train}}^{(\gamma)}$ and training targets $\mathbf{Y}_{\text{train}}^{(\gamma)}$, conditioned on parking type $\gamma \in \Gamma_{\text{type}}$. The training data are concatenated using $\tilde{\mathcal{X}}_{\text{rs}}^{\hat{p}}$, $\tilde{\mathcal{X}}_0^{\hat{p}}$ collected in parking environments from set $\mathbb{E}_{\gamma} \subset \mathbb{E}$, where all the environments share the same parking type γ . Denote \mathcal{E}_i as the i -th element in \mathbb{E}_{γ} , $N_{\mathcal{E}_i}$ as the size of $\tilde{\mathcal{X}}_0^{\hat{p}}[\mathcal{E}_i]$ (or equivalently, the size of $\tilde{\mathcal{X}}_{\text{rs}}^{\hat{p}}[\mathcal{E}_i]$), and the number of environment configurations in \mathbb{E}_{γ} as $|\mathbb{E}_{\gamma}|$. Let $\mathcal{E}'_i = [W_{\text{lane}}^{(i)}, W_{\text{spot}}^{(i)}, D_{\text{deadend}}^{(i)}]$ be the vector of \mathcal{E}_i excluding parking type γ , and $\mathbf{1}_{N_{\mathcal{E}_i}}$ be the $N_{\mathcal{E}_i}$ -dimensional vector of ones, we get

$$\mathbf{X}_{\text{train}}^{(\gamma)} = \begin{bmatrix} \tilde{\mathcal{X}}_0^{\hat{p}}[\mathcal{E}_1] & \mathbf{1}_{N_{\mathcal{E}_1}} \mathcal{E}'_1{}^{\top} \\ \tilde{\mathcal{X}}_0^{\hat{p}}[\mathcal{E}_2] & \mathbf{1}_{N_{\mathcal{E}_2}} \mathcal{E}'_2{}^{\top} \\ \vdots & \vdots \\ \tilde{\mathcal{X}}_0^{\hat{p}}[\mathcal{E}_{|\mathbb{E}_{\gamma}|}] & \mathbf{1}_{N_{\mathcal{E}_{|\mathbb{E}_{\gamma}|}}} \mathcal{E}'_{|\mathbb{E}_{\gamma}|}{}^{\top} \end{bmatrix}, \quad \mathbf{Y}_{\text{train}}^{(\gamma)} = \begin{bmatrix} \tilde{\mathcal{X}}_{\text{rs}}^{\hat{p}}[\mathcal{E}_1] \\ \tilde{\mathcal{X}}_{\text{rs}}^{\hat{p}}[\mathcal{E}_2] \\ \vdots \\ \tilde{\mathcal{X}}_{\text{rs}}^{\hat{p}}[\mathcal{E}_{|\mathbb{E}_{\gamma}|}] \end{bmatrix}.$$

In this work we adopted popular machine learning algorithms of K-Nearest Neighbors (KNN) and Multi-Layer Perceptron (MLP) to train the preparatory pose selector. More advanced models such as deep neural networks and transformers are not used, as our dataset is small and the input is low-dimensional (6D), making simpler models more data-efficient, less prone to overfitting, and sufficient for capturing the underlying structure. We select KNN because it can ensure the output of the learned model $\mathbf{g}_{\text{pre}}^{\hat{p}} \in \mathcal{P}(\mathbf{g}^{\hat{p}}, \mathcal{E})$, where $\mathcal{P}(\mathbf{g}^{\hat{p}}, \mathcal{E})$ is the collection of all states $\mathbf{x}^{\hat{p}} \in \mathbb{R}^3$ that have at least one collision-free RS path to the target parking pose $\mathbf{g}^{\hat{p}}$ in the parking environment \mathcal{E} . Such guarantees can be achieved when KNN uses one neighbor when making the prediction, because the output $\mathbf{g}_{\text{pre}}^{\hat{p}}$ will then be from one of the RS path starting poses $\tilde{\mathcal{X}}_{\text{rs}}^{\hat{p}}$ collected offline. Even though MLP cannot theoretically ensure $\mathbf{g}_{\text{pre}}^{\hat{p}} \in \mathcal{P}(\mathbf{g}^{\hat{p}}, \mathcal{E})$, we select this algorithm for our learning-based methods due to its ability to model complex nonlinear relationships and memory efficiency in comparison to KNNs.

VI. ONLINE EXECUTION FRAMEWORK OF N3P

During online execution, the ego vehicle’s initial state \mathbf{x}_0 , target pose \mathbf{g} , and obstacle point clouds are first transformed into the parking-spot-based frame \hat{p} . In this frame, the relative positions of the drive lane, parking spot, and dead-end boundaries are fixed, allowing a simple brute-force geometric grouping of obstacle points into top, bottom-left, and bottom-right regions to extract the environment

parameters \mathcal{E} . Although not optimal, this approach is fast, straightforward, and sufficient for real-time deployment. More sophisticated abstraction methods could be developed as future work without altering the N3P framework. Finally, the continuous environment \mathcal{E} is matched to the closest discrete configuration $\mathcal{E}_{\text{train}}$ from the offline dataset using

$$\begin{aligned} \mathcal{E}_{\text{train}}(\mathcal{E}) &= \{W'_{\text{lane}}, W'_{\text{spot}}, D'_{\text{deadend}}, \gamma\}, \\ D'_{\text{deadend}} &= \min \left(\left\lfloor \frac{D_{\text{deadend}}}{\Delta d} \right\rfloor \cdot \Delta d, d_{\text{max}} \right), \\ W'_{\text{spot}} &= \min \left(\left\lfloor \frac{W_{\text{spot}}}{\Delta w^{(s)}} \right\rfloor \cdot \Delta w^{(s)}, w_{\text{max}}^{(s)} \right), \\ W'_{\text{lane}} &= \min \left(\left\lfloor \frac{W_{\text{lane}}}{\Delta w^{(l)}} \right\rfloor \cdot \Delta w^{(l)}, w_{\text{max}}^{(l)} \right), \end{aligned} \quad (7)$$

where $w_{\text{max}}^{(s)}, w_{\text{max}}^{(l)}, d_{\text{max}}, \Delta w^{(s)}, \Delta w^{(l)}$, and Δd are defined as in Eq. 4. The online execution framework of N3P is presented in algorithm 1, where $\text{Planner}(\cdot)$ denotes a graph-search or optimization-based parking planner of choice. Instead of $\text{RS}(\cdot)$, we employ Hybrid A* augmented with RS curves, denoted as $\text{HARS}(\cdot)$, to generate a collision-free path from the predicted preparatory pose to the parking goal. This choice is necessary because some learning models (e.g., MLP) do not guarantee that $\mathbf{g}_{\text{pre}}^{\hat{p}} \in \mathcal{P}(\mathbf{g}^{\hat{p}}, \mathcal{E})$, and additional node expansions may be required to ensure feasibility.

Algorithm 1: Learning-based N3P Framework

Input: $\mathcal{E} = \{W_{\text{lane}}, W_{\text{spot}}, D_{\text{deadend}}, \gamma\}$, $\mathbf{x}_0^{\hat{p}}$,
model $f_r(\cdot)$

Output: path

- 1 Compute $\mathcal{E}_{\text{train}}(\mathcal{E})$; // Eq. 7
 - 2 $\mathbf{x} = [x_0^{\hat{p}}, y_0^{\hat{p}}, \theta_0^{\hat{p}}, W_{\text{lane}}, W_{\text{spot}}, D_{\text{deadend}}]^{\top}$;
 - 3 $\mathbf{g}_{\text{pred}}^{\hat{p}} = f_{\gamma}(\mathbf{x}; \mathbf{w})$;
 - 4 path = $\text{Planner}(\mathbf{x}_0^{\hat{p}}, \mathbf{g}_{\text{pred}}^{\hat{p}}, \mathcal{E})$;
 - 5 rsPath = $\text{HARS}(\mathbf{g}_{\text{pred}}^{\hat{p}}, \mathbf{g}^{\hat{p}}(\gamma), \mathcal{E})$;
 - 6 path = path + rsPath;
 - 7 **return** path
-

VII. EXPERIMENT

A. Baselines

To validate the effectiveness of the proposed three-stage parking scheme, we integrate the framework with conventional RS-path-enhanced Hybrid A* algorithms using the MLP and KNN models. The resulting N3P-based Hybrid A* variants (KNN-N3P and MLP-N3P) are evaluated against multiple standard Hybrid A* baselines, including Hybrid A* (HA*), Hybrid A* augmented with the RS model (HA* with RS) [5], Hybrid A* with RS curves returning the best path after evaluating five solutions (HA* Hold), Scenario-based Hybrid A* (SHA*, applicable only in parallel parking scenarios) [8], and Multi-Heuristic Hybrid A* (MHHA*) [9]. To ensure fairness, all Hybrid A* methods employ a heuristic derived from a prior A* cost-to-go computation. The

time required to compute this A* cost-to-go via dynamic programming is included in the reported runtime of Hybrid A. To further demonstrate the advantages of N3P-enhanced Hybrid A* over contemporary autonomous parking agents trained with reinforcement learning (RL), we compared it to HOPE [23], a recent transformer-based RS-path-enhanced RL network for autonomous parking applications. RL-based path planners are known to struggle with generalization beyond their training distribution, with performance highly dependent on the similarity between training and testing environments. To account for this, we train two HOPE variants: one in the simplified environment adopted by N3P for offline data generation (RL-Simple), and the other in the evaluation environment (RL-Eval). Both agents are trained using SAC policies for 10,000 episodes.

B. Evaluation Environment

In contrast to the training environment, which disregards other vehicles in the parking lot and assumes perfect rectangular parking infrastructure, our testing environments randomly place vehicles in neighboring spots and along the drive lane, and introduce dead-end parking layouts that limit the ego vehicle’s maneuvering to evaluate generalization, as in Fig. 5. We do not consider scenarios in which other vehicles completely block the path from the ego vehicle’s starting position to the target spot, as such situations would make the parking task unsolvable for all methods—both in simulation and in real life.

Following Los Angeles’ legal regulations for new parking facilities [29], we specify the size of the target parking spot to fall within the following range: $W_{\text{spot}} \in [2.3, 4.3]$ m for perpendicular (forward and reverse) parking and $W_{\text{spot}} \in [6.0, 8.0]$ m for parallel parking. The driveway width W_{lane} is set to be 6 meters, and the dead end length $D_{\text{deadend}} \in [4.0, 12.0]$ m for all simulations. We model the ego vehicle based on the 2024 Honda Accord [30], setting vehicle length $l_{\text{car}} = 4.97$ m, vehicle width $w = 1.86$ m, wheelbase $l = 2.83$ m, and steering angle δ limit to be 34.9 degrees. We constrain the linear speed for the vehicle to be 2 m/s when moving forward and 1 m/s when moving backward to encourage caution. All simulations are conducted on a 12th Gen Intel® Core™ i7-12700K \times 20. To better evaluate our approaches, we categorize parking scenarios into three difficulty levels:

Easy: Parallel parking $W_{\text{spot}} \in [7.0, 8.0]$ m, bay parking $W_{\text{spot}} \in [3.2, 4.2]$ m; 50% chance of a dead-end wall located 8–12 m from the parking spot center.

Complex: Parallel parking $W_{\text{spot}} \in [6.5, 7.5]$ m, bay parking $W_{\text{spot}} \in [2.8, 3.7]$ m; always includes a dead-end wall located 8–12 m from the parking spot center.

Extreme: Parallel parking $W_{\text{spot}} \in [6.0, 7.0]$ m, bay parking $W_{\text{spot}} \in [2.3, 3.2]$ m; always includes a dead-end wall located 4–8 m from the parking spot center.

C. Comparison and Analysis

The performance of N3P-enhanced Hybrid A* and the baseline planners was evaluated over 100 randomly generated scenarios for each difficulty level and parking type

TABLE I: Validate N3P-Enhanced Hybrid A*'s Performance with Difficulty Level Extreme

	Method	$\min(T)$	\bar{T}	$\text{median}(T)$	$P95(T)$	$\bar{\Delta\delta}$	\bar{L}	Fail %	\bar{N}_{dc}	$\max(N_{dc})$	\bar{N}_{node}
Forward	HA*	1.6911	39.69	36.63	82.46	0.033	17.08	1	1.87	5	18674
	HA* with RS	0.0359	59.45	60.05	120.0	0.029	18.04	0	1.90	5	6875
	HA* Hold	0.4297	77.16	80.24	141.9	0.027	17.61	0	1.65	3	9122
	MHHA*	0.0366	57.87	57.05	113.3	0.030	18.59	0	2.05	5	6635
	RL Simple	0.0720	0.994	0.674	2.854	0.339	31.36	60	31.6	149	75
	RL Eval	0.0987	0.713	0.411	2.277	0.572	26.41	7	26.8	324	55
	MLP-N3P	0.0544	5.178	0.107	32.71	0.033	17.88	0	2.06	7	657
	KNN-N3P	0.0400	1.590	0.092	0.891	0.031	17.54	0	2.03	4	203
Parallel	HA*	17.812	99.77	97.60	152.7	0.027	22.03	9	2.55	6	57261
	HA* with RS	0.0886	16.06	11.55	53.36	0.033	20.78	0	2.02	5	2248
	HA* Hold	0.1392	21.95	16.79	65.38	0.033	20.49	0	2.02	5	3117
	MHHA*	0.0902	14.00	9.422	48.46	0.034	20.78	0	2.04	5	1984
	SHA*	0.0902	11.72	4.696	56.60	0.032	21.31	0	2.03	5	1678
	RL Simple	0.1237	0.734	0.417	3.333	0.307	34.76	16	31.58	332	54
	RL Eval	0.0983	0.309	0.268	0.480	0.381	19.70	0	8.46	80	24
	MLP-N3P	0.0556	1.531	0.111	0.711	0.031	22.03	0	2.82	6	260
KNN-N3P	0.0423	0.675	0.096	0.440	0.030	22.01	0	2.68	5	91	
Reverse	HA*	10.664	36.47	36.33	57.70	0.020	18.78	23	1.08	3	17027
	HA* with RS	0.2166	6.808	4.916	17.72	0.023	19.39	0	1.08	3	1023
	HA* Hold	0.5162	8.983	6.15	24.87	0.023	19.24	0	1.08	3	1394
	MHHA*	0.1460	6.408	4.447	20.55	0.024	19.33	0	1.10	3	954
	RL Simple	0.0748	0.768	0.222	3.633	0.178	31.17	51	29.04	265	50
	RL Eval	0.0879	0.377	0.324	0.591	0.213	24.07	2	12.0	130	29
	MLP-N3P	0.0568	0.424	0.097	0.750	0.023	18.71	2	1.09	3	45
	KNN-N3P	0.0426	0.297	0.078	0.188	0.023	18.52	0	1.05	3	29

TABLE II: Validate N3P-Enhanced Hybrid A*'s Performance with Difficulty Level Complex

	Method	$\min(T)$	\bar{T}	$\text{median}(T)$	$P95(T)$	$\bar{\Delta\delta}$	\bar{L}	Fail %	\bar{N}_{dc}	$\max(N_{dc})$	\bar{N}_{node}
Forward	HA*	1.231	31.23	26.65	70.07	0.031	14.66	1	1.20	4	15274
	HA* with RS	0.0367	22.95	7.630	78.89	0.030	15.44	0	1.42	5	2678
	HA* Hold	0.0977	36.07	21.21	94.36	0.026	14.78	0	0.99	5	4273
	MHHA*	0.0370	21.60	9.120	72.74	0.033	15.56	0	1.56	5	2489
	RL Simple	0.0257	1.298	0.537	4.318	0.359	43.78	58	43.19	301	84
	RL Eval	0.1234	0.802	0.393	3.749	0.548	27.43	9	27.96	252	57.3
	MLP-N3P	0.0591	1.382	0.099	1.436	0.032	15.88	0	1.89	3	179
	KNN-N3P	0.0474	0.092	0.085	0.161	0.031	15.38	0	1.67	2	4
Parallel	HA*	6.4502	83.98	84.20	153.1	0.026	18.90	5	2.04	4	49973
	HA* with RS	0.0294	2.417	0.981	9.100	0.031	18.21	0	1.80	3	312
	HA* Hold	0.0535	3.958	2.118	12.92	0.031	17.90	0	1.78	3	518
	MHHA*	0.0298	1.556	0.821	5.612	0.032	18.32	0	1.79	3	207
	SHA*	0.0312	0.878	0.484	2.597	0.029	19.10	0	1.82	3	107
	RL Simple	0.2046	0.855	0.460	3.572	0.320	37.31	16	36.80	341	62.87
	RL Eval	0.1537	0.294	0.269	0.461	0.383	19.37	0	7.73	24	22
	MLP-N3P	0.0657	0.122	0.101	0.253	0.029	21.07	2	2.04	5	12
KNN-N3P	0.0506	0.090	0.082	0.153	0.030	20.52	0	1.99	3	9	
Reverse	HA*	26.428	53.17	51.68	78.50	0.020	18.33	9	1.00	1	25927
	HA* with RS	0.0632	1.750	0.969	6.435	0.023	18.43	0	1.00	1	242
	HA* Hold	0.1667	2.708	1.828	7.929	0.023	18.27	0	1.00	1	372
	MHHA*	0.0558	1.490	0.938	5.145	0.024	18.48	0	1.00	1	210
	RL Simple	0.0961	0.560	0.234	2.019	0.182	24.74	54	16.4	282	34
	RL Eval	0.1035	0.410	0.352	0.854	0.210	23.95	1	12.1	83	29
	MLP-N3P	0.0622	0.109	0.101	0.141	0.024	19.59	3	1.02	3	5
	KNN-N3P	0.0439	0.086	0.085	0.117	0.023	19.87	0	1.00	1	5

TABLE III: Validate N3P-Enhanced Hybrid A*'s Performance with Difficulty Level Easy

	Method	$\min(T)$	\bar{T}	$\text{median}(T)$	$P95(T)$	$\bar{\Delta\delta}$	\bar{L}	Fail %	\bar{N}_{dc}	$\max(N_{dc})$	\bar{N}_{node}
Forward	HA*	0.2847	19.09	7.898	60.62	0.025	13.43	1	0.77	2	9751
	HA* with RS	0.0342	9.136	0.763	56.32	0.023	15.24	0	1.21	5	1112
	HA* Hold	0.0787	16.17	2.691	74.91	0.022	14.39	0	0.81	4	1991
	MHHA*	0.0345	7.229	0.703	37.19	0.027	15.78	0	1.42	5	859
	RL Simple	0.0463	0.718	0.561	1.860	0.381	28.17	62	23.7	107	49
	RL Eval	0.1001	0.751	0.434	2.500	0.582	25.99	7	24.9	263	53.3
	MLP-N3P	0.0640	0.406	0.097	1.084	0.030	14.81	3	1.51	4	45
	KNN-N3P	0.0490	0.081	0.078	0.153	0.027	13.86	0	1.06	3	3
Parallel	HA*	6.7685	62.49	58.59	126.4	0.027	16.73	10	1.56	4	37502
	HA* with RS	0.0325	0.439	0.291	1.128	0.023	19.17	0	1.35	3	62
	HA* Hold	0.0640	0.974	0.562	4.239	0.024	18.11	0	1.19	2	132
	MHHA*	0.0320	0.432	0.292	1.256	0.025	18.97	0	1.40	3	63
	SHA*	0.0316	0.292	0.160	1.191	0.022	20.08	0	1.34	3	37
	RL Simple	0.1575	0.655	0.449	1.635	0.322	33.32	18	27.1	284	47.99
	RL Eval	0.0994	0.328	0.322	0.465	0.441	21.10	1	8.88	17	25
	MLP-N3P	0.0685	0.143	0.098	0.197	0.028	19.87	8	1.61	5	14
KNN-N3P	0.0514	0.085	0.082	0.140	0.028	19.71	0	1.58	4	6	
Reverse	HA*	30.118	56.75	52.69	86.40	0.020	18.28	10	1.00	1	30739
	HA* with RS	0.0599	0.523	0.325	1.851	0.023	17.60	0	1.00	1	82
	HA* Hold	0.1018	1.124	0.792	3.292	0.023	17.56	0	1.00	1	166
	MHHA*	0.0477	0.552	0.306	1.792	0.024	17.87	0	1.00	1	88
	RL Simple	0.0986	0.695	0.244	2.096	0.146	25.39	53	20.2	195	43
	RL Eval	0.0990	0.358	0.336	0.644	0.201	22.67	3	10.42	38	26
	MLP-N3P	0.0617	0.106	0.099	0.163	0.025	18.68	2	1.05	2	5
	KNN-N3P	0.0471	0.081	0.079	0.111	0.024	19.40	0	1.04	3	5

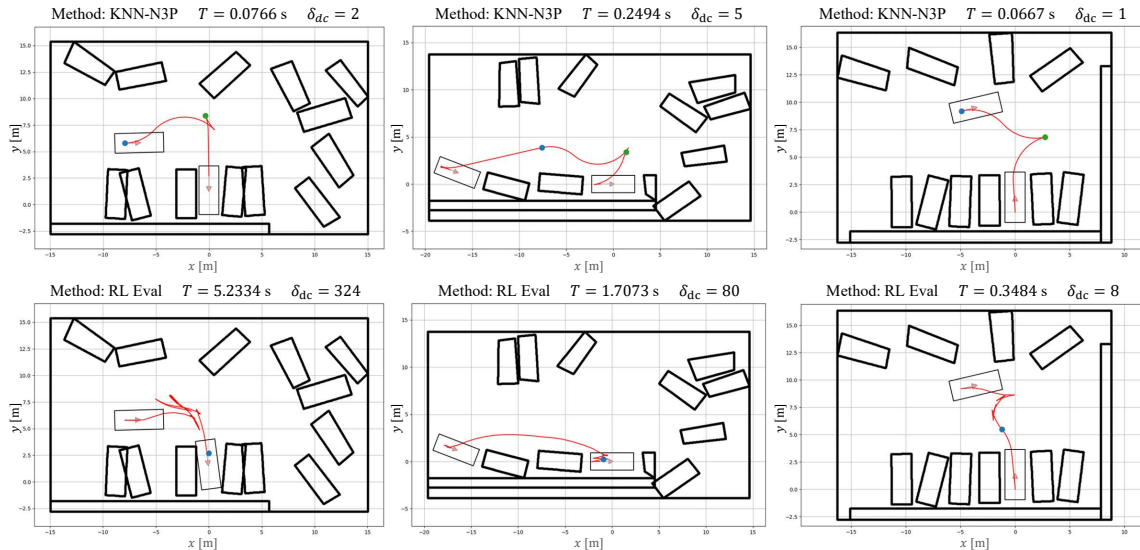


Fig. 5: Comparison of KNN-N3P (top) and the RL agent trained on the evaluation environment (bottom) in forward, parallel, and reverse parking scenarios at the Extreme difficulty level. Red lines indicate the generated trajectories.

(forward, reverse, and parallel) and summarized in Table I, Table II, and Table III. Here, $\min(T)$, \bar{T} , $\text{median}(T)$, and $P95(T)$ denote the minimum, mean, median, and 95th percentile computation times (in seconds), respectively. $\overline{\Delta\delta} = \frac{1}{T} \sum_{i=1}^T \Delta\delta_t$ is the average steering change (in radians), where $\Delta\delta_t = \delta_{t+1} - \delta_t$. \bar{L} is the average trajectory length (in meters). “Fail %” indicates the proportion of trials where a feasible path could not be found. \bar{N}_{dc} and $\max(N_{dc})$ are the average and maximum number of direction changes per trajectory, while \bar{N}_{node} represents the average number of nodes expanded before finding a feasible path. For baselines, it counts expansions toward the goal (or until a RS connection is found). For N3P, it counts expansions toward the predicted preparatory pose, including any extra needed for MLP-N3P to connect the preparatory pose and the goal. For RL agents, it equals the number of executed control steps. Existing RL-based parking planners are typically designed as reactive controllers: they do not plan the full trajectory, but instead select only the next action based on the current vehicle state and environment observations. Therefore, in this work, we measure the computation time for RL agents as the time required to generate successive actions until a feasible RS path to the target can be computed or the vehicle reaches a pose with at least 90% overlap with the target.

The feedforward MLP used in N3P comprises of four hidden layers (256–256–256–128 units with ReLU activations) and requires 50–83 minutes to train, depending on the scenario, whereas the KNN model trains in under 1 second, since it does not involve iterative parameter optimization. However, the MLP is significantly more memory-efficient (655 KB vs. 47.8 MB for KNN). N3P-enhanced Hybrid A* achieves median runtime below 10 Hz and 95th-percentile runtime around 6 Hz in environments of difficulty Complex or Easy, demonstrating low-latency capability in most practical parking scenarios. MLP-N3P runs slightly slower than KNN-N3P and exhibits a non-zero failure rate

because it cannot guarantee $g_{pre}^{\hat{p}} \in \mathcal{P}(g^{\hat{p}}, \mathcal{E})$. Consequently, the predicted preparatory pose may occasionally collide with obstacles or fail to admit a direct RS connection, requiring additional node expansions; in such cases, reverting to the default Hybrid A* planner ensures feasibility. Overall, KNN is the more favorable choice for training model.

Compared to existing Hybrid A* variants, KNN-N3P and MLP-N3P reduce average runtime by 86.1–93.6% and 89.7–99.5%, respectively, relative to the fastest graph-search baseline. N3P maintains nearly unchanged trajectory lengths, with only moderate increases in direction changes for forward and parallel parking, while matching the best baseline in reverse parking across all difficulty levels. Only small increases in average steering variation $\Delta\delta$ are observed, ranging from 0.003–0.006 rad per trajectory. The RL agent trained in the same abstracted environment as N3P fails to generalize to evaluation scenarios, with failure rates of 16–60%, primarily due to distributional shifts between training and testing settings. The RL agent trained directly in the evaluation environment performs better, achieving 0% failure in parallel parking and below 2% in reverse parking, consistent with the original report [23]. However, in forward parking scenarios not explicitly considered in the original work, the failure rate rises to 9%. Beyond failures, RL agents also underperform in trajectory quality. We observe a roughly 10× increase in average steering variation $\overline{\Delta\delta}$ and direction changes \bar{N}_{dc} , as the agent attempts to maneuver into the parking spot without an effective preparatory pose (see Fig. 5). Across average, median, and 95th-percentile metrics, RL trajectories are consistently slower than those produced by N3P, except in extreme parallel parking scenarios. These results demonstrate that N3P outperforms RL-based planners in both reliability and path quality.

VIII. CONCLUSION, LIMITATIONS & FUTURE WORK

This work introduces the N3P framework to accelerate traditional autonomous parking path planning problems. The

N3P-enhanced Hybrid A* successfully reduces runtime of Hybrid A* variants by 86% while maintaining comparable trajectory quality. These results demonstrate that incorporating naturalistic maneuver decomposition into structured planning frameworks offers a principled alternative to purely learned parking policies.

However, several limitations remain. The environment abstraction can produce suboptimal solutions, particularly in cases such as dead ends inclined toward the target parking spot, where the preparatory pose predictor may underestimate the feasible region. The KNN preparatory pose predictor achieves 100% feasibility in noise-free simulations. In real-world settings, feasibility holds when abstracted environment parameters are no larger than ground truth, motivating the use of a safety margin to account for measurement noise. For parallel parking of difficulty level Extreme, runtime reduction fails in 1–2 out of 100 cases, typically when the target spot is adjacent to a dead-end wall with tight constraints on the opposite lane side. These edge cases suggest the need for a more expressive preparatory pose selector with richer environment parameterization for parallel parking scenarios with tight dead ends. Finally, the framework relies on vehicle-specific offline data and requires retraining when vehicle dimensions change. Future work will address cross-vehicle generalization, improved environment abstraction, and extension to angled parking.

REFERENCES

- [1] Liping Cheng, Chuanxi Liu, and Bo Yan. Improved hierarchical a-star algorithm for optimal parking path planning of the large parking lot. In *2014 IEEE international conference on information and automation (ICIA)*, pages 695–698. IEEE, 2014.
- [2] Long Han, Quoc Huy Do, and Seiichi Mita. Unified path planner for parking an autonomous vehicle based on rrt. In *2011 IEEE International Conference on Robotics and Automation*, pages 5622–5627. IEEE, 2011.
- [3] Peter E. Hart, Nils J. Nilsson, and Bertram Raphael. A formal basis for the heuristic determination of minimum cost paths. *IEEE Transactions on Systems Science and Cybernetics*, 4(2):100–107, 1968.
- [4] Steven LaValle. Rapidly-exploring random trees: A new tool for path planning. *Research Report 9811*, 1998.
- [5] Dmitri Dolgov, Sebastian Thrun, Michael Montemerlo, and James Diebel. Practical search techniques in path planning for autonomous driving. *ann arbor*, 1001(48105):18–80, 2008.
- [6] Héctor J Sussmann and Guoqing Tang. Shortest paths for the reeds-shepp car: a worked out example of the use of geometric techniques in nonlinear optimal control, 1991.
- [7] Ibrahim Ibrahim, Wilm Decré, and Jan Swevers. Accelerated reeds–shepp and underspecified reeds–shepp algorithms for mobile robot path planning. *IEEE Transactions on Robotics*, 41:2691–2708, 2025.
- [8] Xuemin Chi, Zhitao Liu, Jihao Huang, Feng Hong, and Hongye Su. Optimization-based motion planning for autonomous parking considering dynamic obstacle: A hierarchical framework. In *2022 34th Chinese Control and Decision Conference (CCDC)*, pages 6229–6234, 2022.
- [9] Jihao Huang, Zhitao Liu, Xuemin Chi, Feng Hong, and Hongye Su. Search-based path planning algorithm for autonomous parking: Multi-heuristic hybrid a. In *2022 34th Chinese Control and Decision Conference (CCDC)*, pages 6248–6253. IEEE, 2022.
- [10] Antonio Acernese, Giulio Borrello, Luca Lorusso, and Michele Basso. Informed hybrid a star-based path planning algorithm in unstructured environments. In *2024 European Control Conference (ECC)*, pages 1039–1044, 2024.
- [11] Xiaojing Zhang, Alexander Liniger, and Francesco Borrelli. Optimization-based collision avoidance. *IEEE Transactions on Control Systems Technology*, 29(3):972–983, 2020.
- [12] Grady Williams, Paul Drews, Brian Goldfain, James M. Rehg, and Evangelos A. Theodorou. Aggressive driving with model predictive path integral control. In *2016 IEEE International Conference on Robotics and Automation (ICRA)*, pages 1433–1440, 2016.
- [13] Chang Liu, Seungho Lee, Scott Varnhagen, and H. Eric Tseng. Path planning for autonomous vehicles using model predictive control. In *2017 IEEE Intelligent Vehicles Symposium (IV)*, pages 174–179, 2017.
- [14] Pei Zhang, SiLong Zhou, Jie Hu, WenLong Zhao, Jiachen Zheng, Zhiling Zhang, and Chongzhi Gao. Automatic parking trajectory planning in narrow spaces based on hybrid a* and nmmpc. *Scientific Reports*, 15(1):1384, 2025.
- [15] Zhouheng Li, Lei Xie, Cheng Hu, and Hongye Su. A rapid iterative trajectory planning method for automated parking through differential flatness. *Robotics and Autonomous Systems*, 182:104816, 2024.
- [16] Zhichao Han, Yuwei Wu, Tong Li, Lu Zhang, Liyao Pei, Long Xu, Chengyang Li, Changjia Ma, Chao Xu, Shaojie Shen, and Fei Gao. An efficient spatial-temporal trajectory planner for autonomous vehicles in unstructured environments. *IEEE Transactions on Intelligent Transportation Systems*, 25(2):1797–1814, 2024.
- [17] Bai Li, Tankut Acarman, Youmin Zhang, Yakun Ouyang, Cagdas Yaman, Qi Kong, Xiang Zhong, and Xiaoyan Peng. Optimization-based trajectory planning for autonomous parking with irregularly placed obstacles: A lightweight iterative framework. *IEEE Transactions on Intelligent Transportation Systems*, 23(8):11970–11981, 2022.
- [18] Runqi Chai, Antonios Tsourdos, Al Savvaris, Senchun Chai, Yuanqing Xia, and CL Philip Chen. Design and implementation of deep neural network-based control for automatic parking maneuver process. *IEEE Transactions on Neural Networks and Learning Systems*, 33(4):1400–1413, 2020.
- [19] Runqi Chai, Derong Liu, Tianhao Liu, Antonios Tsourdos, Yuanqing Xia, and Senchun Chai. Deep learning-based trajectory planning and control for autonomous ground vehicle parking maneuver. *IEEE Transactions on Automation Science and Engineering*, 20(3):1633–1647, 2022.
- [20] Dongchan Kim and Kunsoo Huh. Neural motion planning for autonomous parking. *International Journal of Control, Automation and Systems*, 21(4):1309–1318, 2023.
- [21] Xu Shen and Francesco Borrelli. Multi-vehicle conflict resolution in highly constrained spaces by merging optimal control and reinforcement learning. *IFAC-PapersOnLine*, 56(2):3308–3313, 2023.
- [22] Runqi Chai, Hanlin Niu, Joaquin Carrasco, Farshad Arvin, Hujun Yin, and Barry Lennox. Design and experimental validation of deep reinforcement learning-based fast trajectory planning and control for mobile robot in unknown environment. *IEEE Transactions on Neural Networks and Learning Systems*, 35(4):5778–5792, 2022.
- [23] Mingyang Jiang, Yueyuan Li, Songan Zhang, Siyuan Chen, Chunxiang Wang, and Ming Yang. Hope: A reinforcement learning-based hybrid policy path planner for diverse parking scenarios. *IEEE Transactions on Intelligent Transportation Systems*, 26(5):6130–6141, 2025.
- [24] Mathias Bos, Bastiaan Vandewal, Wilm Decré, and Jan Swevers. Mpc-based motion planning for autonomous truck-trailer maneuvering. *IFAC-PapersOnLine*, 56(2):4877–4882, 2023. 22nd IFAC World Congress.
- [25] Yaogang Zhang, Guoying Chen, Hongyu Hu, and Zhenhai Gao. Hierarchical parking path planning based on optimal parking positions. *Automotive Innovation*, 6(2):220–230, 2023.
- [26] Rajesh Rajamani. *Vehicle dynamics and control*. Springer, 2006.
- [27] Saied Sedighi, Duong-Van Nguyen, and Klaus-Dieter Kuhnert. Guided hybrid a-star path planning algorithm for valet parking applications. In *2019 5th International Conference on Control, Automation and Robotics (ICCAR)*, pages 570–575, 2019.
- [28] James Reeds and Lawrence Shepp. Optimal paths for a car that goes both forwards and backwards. *Pacific journal of mathematics*, 145(2):367–393, 1990.
- [29] Los angeles municipal code §12.21(a)(1): Parking stall dimensions. https://codelibrary.amlegal.com/codes/los_angeles/latest/lapz/0-0-0-5183. Accessed: Jan. 2026.
- [30] American Honda Motor Co., Inc. 2024 honda accord: Specifications & features (press release), 2024. Accessed: Oct. 31, 2025.